A role for phylloquinone biosynthesis in the plasma membrane as revealed in a non-photosynthetic parasitic plant

Xi Gu[1], Scott A. Harding[2], Batbayar Nyamdari[2], Kavita B. Aulakh[2], Kristen Clermont[3], James H. Westwood[3], Chung-Jui Tsai[1,2,*]

[1]Institute of Bioinformatics, University of Georgia, Athens, GA 30602, USA.

[2]School of Forestry and Natural Resources, Department of Genetics, and Department of Plant Biology, University of Georgia, Athens, GA 30602, USA.

[3]Department of Plant Pathology, Physiology, and Weed Science, Virginia Polytechnic Institute and State University, Blacksburg, VA 24061, USA.

*Correspondence to: cjtsai@uga.edu

Phylloquinone (PhQ) is found predominantly in thylakoid membranes of photosynthetic tissues where it functions in photosystem I electron transport. PhQ has also been detected in plasma membranes, but neither the molecular basis nor the significance of this non-canonical pathway has been elucidated. Here we provide evidence of plasma membrane PhQ biosynthesis in a non-photosynthetic holoparasite *Phelipanche aegyptiaca*. A non-photosynthetic role is supported by transcription of the entire suite of PhQ biosynthetic genes, plasma membrane-localization of the terminal enzymes, and detection of PhQ in *Phelipanche* seeds. Analysis of PhQ-coexpressed genes in the holoparasite revealed increased cellular commitment to oxidation-reduction and defense relative to photosynthetic parasites. Coexpression network inference identified oxidoreductases involved in plasma membrane electron transport, implicating PhQ in a transmembrane redox relay associated with parasitism. Plasma membrane PhQ biosynthesis is also predicted to occur in photoautotrophic taxa via alternative splicing, suggesting non-plastidial PhQ is evolutionarily conserved.

Phylloquinone (PhQ or vitamin K1) is a membrane-bound naphthoquinone derivative well-characterized for its role in photosynthetic electron transport (*1*). Accordingly, PhQ is found predominantly in thylakoids, and PhQ-deficient *Arabidopsis thaliana* mutants are seedling-lethal or growth-impaired due to reduced photosystem I (PSI) function (*2*). PhQ has recently emerged as a redox partner in oxidative protein folding in both cyanobacteria and plants (*3, 4*). PhQ has also been detected in plasma membrane (PM) preparations of maize roots, raising the possibility that PhQ may function in transmembrane electron transport similar to its eubacterial counterpart menaquinone (*5, 6*). However, molecular evidence in support of PM-PhQ biosynthesis remains elusive.

The PhQ biosynthetic pathway has an endosymbiotic origin, comprising a series of "Men" proteins named after their eubacterial homologs (*2*). We have observed in multiple photosynthetic taxa that PhQ pathway genes have measurable expression in heterotrophic tissues. However, disentangling the non-photosynthetic function of PhQ from its canonical role has been challenging, due to difficulty in ascertaining heterotrophic state. We therefore exploited parasitic

plants as a study system, reasoning that PhQ biosynthesis in an obligate, non-photosynthetic parasite, if substantiated, would facilitate investigation of PhQ functions outside PSI. We mined the transcript assemblies from the Parasitic Plant Genome Project (*7*), covering the full range of photosynthetic capacities in the Orobanchaceae family, including an obligate holoparasite *Phelipanche aegyptiaca*, an obligate hemiparasite *Striga hermonthica*, and a facultative hemiparasite *Triphysaria versicolor*. Full-length coding sequences were identified for *ICS* and *MenE* genes in *P. aegyptiaca*, along with partial assemblies of other PhQ pathway genes. Fragmented transcripts may represent nonfunctional relics of genes undergoing degeneration, or may reflect technical limitations of *de novo* assembly that prevented identification of the full complement of PhQ biosynthetic genes.

We addressed the fragmented assembly challenge by developing PLAS (Parallelized Local Assembly of Sequences), a pipeline that combines reference-guided mapping (against the *Mimulus* proteome in this case) with iterative *de novo* assembly for transcriptome reconstruction. When applied to the parasitic RNA-seq datasets, we successfully recovered full-length transcripts for all PhQ genes with intact ORFs from the holoparasite (data S1). These transcripts showed moderate to high abundances during *P. aegyptiaca* development (Fig. 1A). Two multifunctional genes recently implicated in PhQ biosynthesis were either poorly expressed (*NAD(P)H DEHYDROGENASE C1*, FPKM<10) or not recovered (*PHYTYL-PHOSPHATE KINASE*). These genes are also involved in the biosynthesis and redox cycle of α-tocopherol (*8, 9*). The interconnection between PhQ biosynthesis and other plastid-derived metabolites (*2*) is therefore absent or reduced in the holoparasite. Among the canonical PhQ biosynthesis genes, *PHYLLO*, *MenE* and *DHNAT* transcripts were detected at similar levels in the three parasites. However, the expression patterns of *ICS*, *MenB*, *MenA* and *MenG* differed between the non-photosynthetic *P. aegyptiaca* and its photosynthetic relatives, especially in response to germination stimulants and haustorium-inducing factors (HIFs) during early development (Fig. 1A). These data strongly support a role for PhQ beyond photosynthesis, and hint at divergent regulation of PhQ biosynthesis associated with photosynthetic and non-photosynthetic functions. HPLC analysis confirmed the presence of PhQ in germinated *P. aegyptiaca* seeds prior to haustorium initiation (Fig. 1B), with an estimated level of 0.05±0.02 pmol/mg dry weight (n=3). For reference, PhQ level in *A. thaliana* seed was 0.12±0.03 pmol/mg dry weight (n=3) (Fig. 1C).

Intracellular compartmentalization is a hallmark of PhQ biosynthesis in plants, with the early and late pathway steps occurring in the plastid, and the intermediate steps in peroxisomes (*10*). We asked whether PhQ biosynthetic enzymes in *P. aegyptiaca* exhibit altered subcellular targeting that would support non-photosynthetic functions. Protein subcellular localization analyses predicted plastid- and peroxisome-targeting of early (PaICS and PaPHYLLO) and intermediate (PaMenE, PaMenB and PaDHNAT) pathway steps, respectively (table S1, figs. S1-S3), similar to their orthologs in photoautotrophic taxa (*2*). However, the predicted polypeptides of terminate enzymes PaMenA and PaMenG were substantially shorter at the N-terminus when compared to their *A. thaliana* orthologs (figs. S4-5). The N-truncated PaMenA and PaMenG scored poorly for plastid-targeting with multiple prediction programs (Fig. 1D), suggesting their non-plastid localization. MenA is a chloroplast envelop enzyme (*11*), consistent with the prediction of AtMenA and PaMenA as integral membrane proteins (Fig. 1E). The absence of an N-terminal plastid-targeting peptide in PaMenA suggests its localization to other membranes. By expressing *35S:PaMenA-GFP* in stably transformed *Nicotiana benthamiana*, we demonstrated PM localization of PaMenA (Fig. 1F). MenG catalyzes the terminal step in thylakoid membranes (*12*). We showed that GFP fused to the N-truncated PaMenG was localized to PM in transgenic

N. benthamiana leaves (Fig. 1G). The PM-localized PaMenA-GFP and PaMenG-GFP signals were distinguishable from tonoplast GFP signals in guard cells and trichomes (fig. S6). The data indicated a redirection of PhQ biosynthesis to PM in the non-photosynthetic *P. aegyptiaca*.

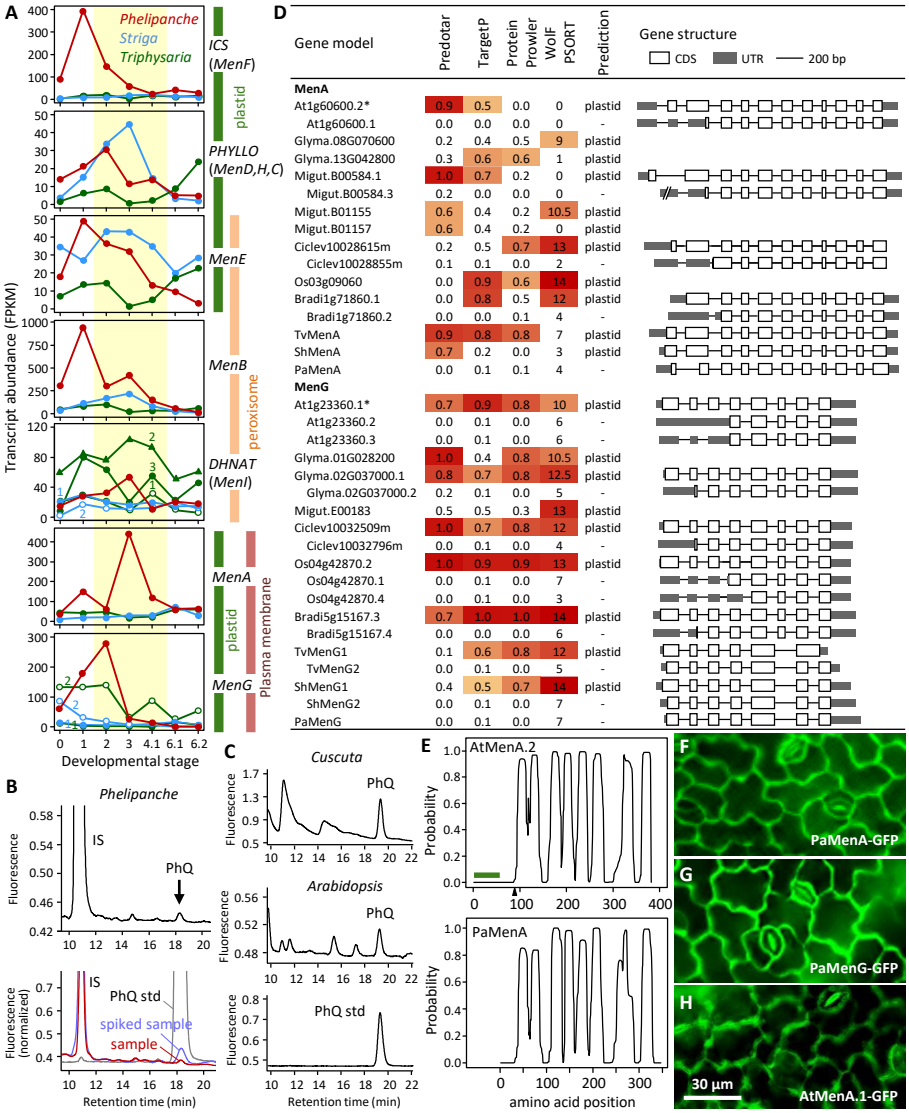

Fig. 1. PhQ biosynthesis in parasitic plants. (**A**) Expression profiles of PhQ biosynthetic genes during parasitic plant development. Genes are ordered according to the pathway, and the predicted protein subcellular localization shown. Developmental stages are as reported (*7*): 0, imbibed seeds; 1, germinated seeds; 2, HIF-treated seedlings; 3, haustoria, pre-vascular connection; 4.1 haustoria, post-vascular connection; 6.1 leaves/stems; 6.2, floral buds. (**B**) HPLC detection of PhQ in germinated *P. aegyptiaca* seeds (top). The lower panel overlays the authentic standard and sample with or without PhQ spike (internal standard, menaquinone). (**C**) PhQ detection in *C. campestris* germinated seeds (top) and *A. thaliana* seeds (middle), in comparison with authentic standard (bottom). (**D**) Plastid-targeting prediction of MenA and MenG polypeptides from various species. Heatmaps show prediction strengths above the 50th percentile of each method, and asterisks denote experimentally verified plastidial proteins. Exon-intron structures are shown for representative genes and their splice variants lacking the transient peptide. (**E**) Transmembrane domain prediction of AtMenA.2 and PaMenA. The green bar in the top panel denotes the plastid transient peptide, and the arrowhead indicates the start of splice variant AtMenA.1. The x-axis in lower panel is shifted for alignment with AtMenA.2. (**F-H**) Plasma membrane localization of GFP fusion with PaMenA (F), PaMenG (G) and AtMenA.1 (H). Additional images from guard cells and trichomes are shown in fig. S6.

To bolster this finding, we mined the 1000 Plants database (*13*), and found that *MenA* transcripts from several other holoparasites, including *Orobanche fasciculata* and *Conopholis americana* of Orobanchaceae, and *Cuscuta campestris* of Convolvulaceae, also lack plastid-targeting sequences (fig. S4). By contrast, the predicted N-termini of MenA from closely-related photosynthetic taxa resemble those of *S. hermonthica* and *T. versicolor* (fig. S4). In the case of MenG, transcripts encoding both long (MenG1) and short (MenG2) isoforms (with or without the plastid transient peptide, respectively) were identified in photosynthetic *S. hermonthica*, *T. versicolor*, and *Kigelia africana*, but only the N-truncated short isoform was found in holoparasites (fig. S5). The two MenG isoforms likely arose from a gene duplication event in the common ancestor of Lamiales. Interestingly, N-truncated *MenG2* was the dominant transcript in both *S. hermonthica* and *T. versicolor* (Fig. 1A). *MenG1* encoding the plastidial isoform was detected at low levels in photosynthetic parasites, and was lost in multiple

holoparasite lineages. PhQ was detected in germinated seed of *C. campestris* (Fig. 1C), at 1.49±0.38 pmol/mg dry weight (n=4). Together, the identification of N-truncated *MenA/MenG* transcripts in unrelated holoparasites, and the detection of PhQ in *P. aegyptiaca*, a root parasite, and *C. campestris*, a stem parasite, lend credence to conserved PM-PhQ biosynthesis in non-photosynthetic parasites.

N-truncated MenA and MenG isoforms are also predicted to occur in *A. thaliana* via alternative splicing, based on the ARAPORT11 genome release (Fig. 1D). The alternative splice junctions of *AtMenA.1* (At1g60600.1), *AtMenG.2* and *AtMenG*.3 (At1g23360.2 and At1g23360.3, with identical coding sequence) were supported by ESTs (GenBank accessions AV832198, AV829761 and AI993608). We surveyed available plant genomes at Phytozome (v11) and identified multiple dicot and monocot species with alternative splicing at both loci that could give rise to N-truncated isoforms with poor plastid-targeting prediction (Fig. 1D). In agreement with the prediction, stable expression of *35S:AtMenA.1-GFP* in transgenic *N. benthamiana* leaves showed localization to PMs (Fig. 1H), instead of plastids as reported for AtmenA.2 (*14*). We interpret the results to suggest that PM-PhQ biosynthesis is evolutionarily conserved in angiosperms. Dual subcellular localization in photosynthetic species is afforded via alternative splicing of the terminal PhQ biosynthetic genes, whereas in non-photosynthetic holoparasites, relaxed selection in plastid-targeting sequences led to degeneration of the transient peptide and PM-targeting of the terminal enzymes. Our data thus provide molecular evidence to corroborate previous detection of PhQ in plant PM preparations (*5*, *6*).

Coexpression analysis revealed high levels of coregulation among PhQ genes in the holoparasite *P. aegyptiaca*, but not in the photosynthetically competent *S. hermonthica* and *T. versicolor*, particularly between early- and late-pathway genes (Fig. 2A-C). Given that PhQ genes were also tightly coregulated in photosynthetic tissues of green plants (fig. S7), lessened co-expression in *S. hermonthica* and *T. versicolor* is consistent with dual involvement of those genes in plastid and PM PhQ biosynthesis. To shed light on PM-PhQ functions, we extracted the top 500 most highly-correlated transcripts for each PhQ gene. The union set contained 2447, 3677 and 3930 unique transcripts for *P. aegyptiaca*, *S. hermonthica* and *T. versicolor*, respectively. The smaller *P. aegyptiaca* dataset is consistent with stronger coexpression of PhQ genes when compared to *S. hermonthica* and *T. versicolor*. Subsets of Gene Ontology (GO)-annotated (Biological Process) transcripts (645, 1199 and 1173 for *P. aegyptiaca*, *S. hermonthica* and *T. versicolor*, respectively) were then subjected to functional enrichment analysis. Transcripts associated with photosynthesis-related processes comprised 3-4% of the GO-annotated transcripts in photosynthetic parasites, but were negligible in *P. aegyptiaca* (Fig. 2D). With the loss of

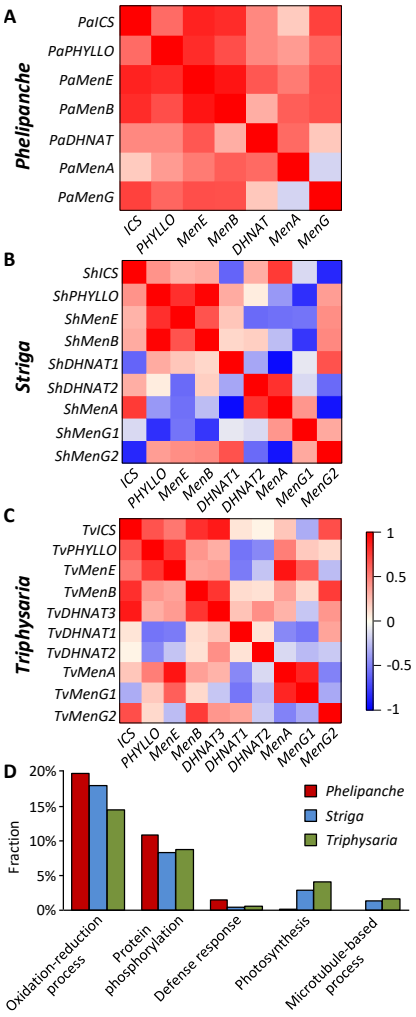

Fig. 2. Coexpression of PhQ genes. (**A-C**) Coexpression patterns among PhQ biosynthesis genes based on Gini correlation coefficient. (**D**) GO enrichments of PhQ-coexpressed genes (union of top 500). Only GO terms with differential enrichment in *P. aegyptiaca* relative to *S. hermonthica* and *T. versicolor* are shown. The distribution of top ten GO terms, and analysis using a correlation coefficient cutoff are shown in fig. S8.

photosynthetic capacity, non-photosynthetic functions of PhQ are expected to become more enriched in *P. aegyptiaca*. We found increased proportions of transcripts associated with oxidation-reduction process, protein phosphorylation and defense response in *P. aegyptiaca* relative to *S. hermonthica* and *T. versicolor* (Fig. 2D). Similar patterns were observed when we used a different criterion (Gini correlation coefficient ≥0.8) to select PhQ-coexpressed transcripts (fig. S8). The increased enrichment of *P. aegyptiaca* PhQ-coexpressed genes in oxidation-reduction and defense-related processes is consistent with PhQ serving as a membrane-bound redox-active cofactor.

We focused on transcripts assigned to oxidation-reduction, defense and photosynthesis GO terms for coexpression network analysis. Inclusion of orthologs from all three species resulted in 359, 544 and 559 non-redundant transcripts from *P. aegyptiaca*, *S. hermonthica* and *T. versicolor*, respectively (data S2). Network visualization of coexpression patterns revealed striking differences. Two dense modules were detected for photosynthetic *S. hermonthica* and *T. versicolor*; one was enriched with photosynthesis genes (Fig. 3A, green nodes) while the other contained known parasitism genes (blue, cyan and magenta nodes, see below). However, only one dense module containing parasitism genes was detected for the non-photosynthetic *P. aegyptiaca*. The PhQ genes (orange nodes) were highly interconnected with parasitism genes in the *P. aegyptiaca* network, but were scattered over the two modules in both *S. hermonthica* and *T. versicolor* networks. We ranked genes by the number of edges they shared with PhQ genes (referred to as k_{PhQ}) in each network, and observed a strong enrichment of PhQ-interconnected genes in the smaller *P. aegyptiaca* network. More than 23% of *P. aegyptiaca* nodes had a k_{PhQ} =4-6 (*i.e.*, connected with a majority of the PhQ genes). However, less than 3% of the *S. hermonthica* and *T. versicolor* nodes met the same criterion (k_{PhQ} ≥5 of 9-10 PhQ genes), and only 10 and 15% of their respective nodes had a k_{PhQ} ≥4 (Fig. 3A, k_{PhQ} bars).

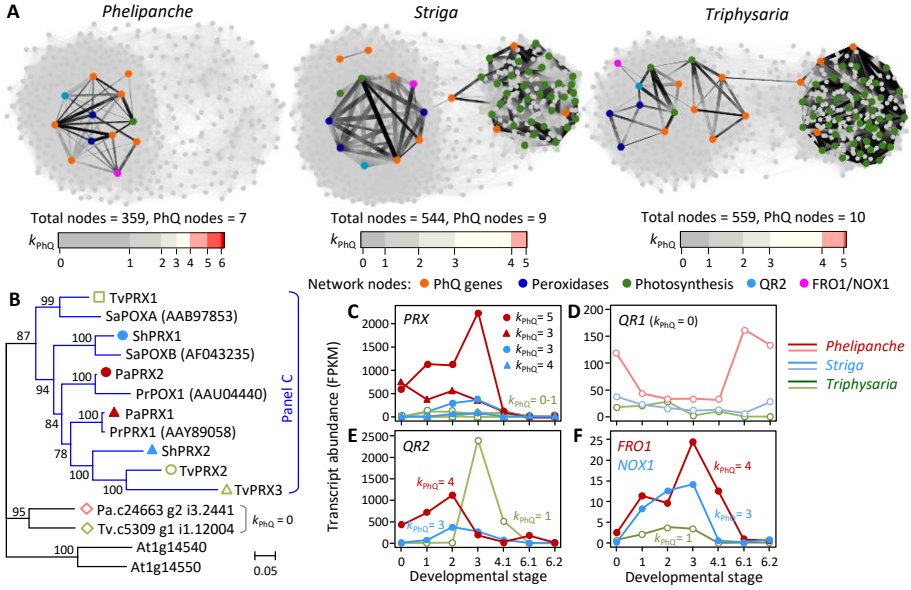

Fig. 3. Network visualization and expression profiles of PhQ-coexpressed genes. (**A**) PhQ-coexpression networks of the parasitic plants. Edge thickness reflects the coexpression strength. Scale bars depict the distribution of nodes according to their connectivity with PhQ genes (k_{PhQ}). (**B**) Bayesian phylogeny of peroxidases (PRX). Orthologs of experimentally characterized PRXs are color-coded by species in the blue clade. (**C-F**) Expression profiles of *PRX* (C), *QR1* (D), *QR2* (E), and *FRO1/NOX1* (F) orthologs. Solid symbols with dark colors denote PhQ-coexpressed genes (k_{PhQ} ≥3), and others are shown in open symbols/light colors. Developmental stages are the same as in Fig. 1.

We validated the *P. aegyptiaca* PhQ network using oxidoreductases known to be involved in parasitism. Several peroxidases, including *SaPOXA* and *SaPOXB* from *S. asiatica* and *PrPOX1* and *PrPRX1* of *P. ramosa*, are specifically expressed in radicles actively secreting peroxidases, and their encoded proteins can oxidize a range of host cell wall-derived phenolics into benzoquinones for haustorium induction (*15-17*). We identified seven corresponding orthologs

from the parasitic species investigated here (Fig. 3B, blue clade). Transcripts of *P. aegyptiaca* orthologs were detected at high levels throughout seed germination and haustorium initiation, in sharp contrast to the patterns observed for *S. hermonthica* and *T. versicolor* orthologs (Fig. 3C). The PhQ-coexpression strength (k_{PhQ}) of these peroxidases was highest in *P. aegyptiaca*, followed by *S. hermonthica*. However, PhQ coexpression was not observed for the *T. versicolor* orthologs, or for orthologs in the neighboring clade of the phylogenetic tree (Fig. 3B). Thus, the PhQ-coexpression of the secretory peroxidases appeared to be positively correlated with parasitism. Another parasitism gene *QR1* encodes an NAD(P)H-dependent quinone reductase, which reduces host-derived quinones into highly reactive semiquinones that have been reported to function in haustorium induction (*18*). *QR1* transcripts were identified in all three parasites, but were not coexpressed with PhQ genes. In *P. aegyptiaca* specifically, *QR1* transcript levels were higher in imbibed than germinated seeds, whereas PhQ gene expression peaked at or after seed germination (Fig. 1A vs. 3D). These findings placed PhQ and PhQ-coexpressed genes downstream of *QR1* in haustorium signaling.

We next explored the *P. aegyptiaca* PhQ subnetwork for redox proteins involved in transmembrane electron flow. Membrane-associated NAD(P)H-oxidoreductases (QRs/NQRs) are an integral component of electron transport (*19, 20*). Two groups of flavin-containing QRs/NQRs are potential candidates, one represented by QR2 (*21*) and its *A. thaliana* orthologs/genome duplicates At5g54500 and At4g27270, and the other by NQR1/At3g27890 (*22*). The parasitic *NQR1* orthologs were not captured in the PhQ networks. However, *QR2* transcripts exhibited strong PhQ-coexpression in *P. aegyptiaca* (k_{PhQ} =4) and *S. hermonthica* (k_{PhQ} =3)(Fig. 3E), in line with *QR2* responsiveness to HIFs during haustorium formation of *Phtheirospermum japonicum* and *S. asiatica* (*23, 24*). These findings, along with the reported PM-association of AtQR2s (*25*), support QR2 involvement in the PM redox system. Membrane-bound NAD(P)H oxidase (NOX) is another key component of the electron transport chain, and partially purified NOX from soybean PMs was shown to catalyze oxidation of reduced PhQ (*26*). Despite this early finding and despite extensive studies of the plant respiratory burst oxidase homologs, identity of the oxidases involved in trans-PM electron transport remains elusive. We found only one *NOX* ortholog in the *S. hermonthica* network (Fig. 3F, k_{PhQ} = 3), and its counterpart in *S. asiatica* (*SaNOX1*) was recently shown to be root-specific and HIF-responsive (*24*). The *P. aegyptiaca* transcriptome lacked *NOX1*, but a ferric-chelate reductase (*PaFRO1*) exhibited strong PhQ-coexpression (k_{PhQ} = 4)(Fig. 3F). Interestingly, *FRO1* transcript was not recovered in the *NOX1*-harboring *S. hermonthica*. FROs are PM-localized flavoproteins involved in electron transfer associated with metal ion homeostasis (*19*). The PhQ-coexpressed *PaFRO1* is orthologous to the *A. thaliana AtFRO4/AtFRO5* tandem duplicates that encode copper-chelate reductases necessary for copper acquisition by root tips (*27*). This suggests that the trans-PM redox system for copper uptake in roots might have been co-opted for parasitic signaling and haustorium development in *P. aegyptiaca*. The FRO1/NOX1 may also facilitate redox exchange for disulfide bond formation in oxidative protein folding (*26*), a process that has been shown to involve PhQ as a cofactor in both plants and cyanobacteria (*3, 4*).

The early stages of parasitic lifecycle can be characterized as a continuum of oxidative events, from perception of host signals and activation of HIFs, to host penetration and vascular connection (*20, 28*). Redox regulation is also integral to defense and to normal development, such as germination, root elongation, and cell wall remodeling (*20*). The redox-active PM-PhQ may function in all of the above processes, but based on the expression profiles of PhQ pathway genes (Fig. 1A), the PM-PhQ most likely participates in the redox relay associated with

haustorium initiation and development. Our observation that many of the PhQ pathway genes and their co-regulated redox proteins exhibited different expression profiles between *P. aegyptiaca* and its photosynthetic relatives underscores the parasitic diversity (*28*), with increased specialization in signaling mechanisms of the holoparasite. Repurposing PhQ for PM-redox signaling during haustorium initiation thus represents another example of parasitic plants adapting common pathways for parasitism.

Beyond potential roles in parasite development and signal transduction, these data demonstrate that PhQ is biosynthesized and functions in non-photosynthetic plants. Given the conservation of PM-PhQ biosynthesis in angiosperms, the existence of alternative functions of PhQ in *P. aegyptiaca* offers an unequivocal basis for identifying non-photosynthetic functions in photoautotrophic species.

1. K. Brettel, P. Sétif, P. Mathis, Flash-induced absorption changes in photosystem I at low temperature: evidence that the electron acceptor A1 is vitamin K1. *FEBS Letters* **203**, 220-224 (1986).
2. J. B. Gilles, L. Scott, F. Abdelhak, S. Eric, B. Anna, Phylloquinone (Vitamin K1): Occurrence, biosynthesis and functions. *Mini-Reviews in Medicinal Chemistry* **16**, 1-11 (2016).
3. F. Furt *et al.*, A bimodular oxidoreductase mediates the specific reduction of phylloquinone (vitamin K1) in chloroplasts. *Plant Journal* **64**, 38-46 (2010).
4. W. Li *et al.*, Structure of a bacterial homologue of vitamin K epoxide reductase. *Nature* **463**, 507-512 (2010).
5. S. Lüthje *et al.*, Quinones in plant plasma membranes — a missing link? *Protoplasma* **205**, 43-51 (1998).
6. K. Lochner, O. Döring, M. Böttger, Phylloquinone, what can we learn from plants? *BioFactors* **18**, 73-78 (2003).
7. Z. Yang *et al.*, Comparative transcriptome analyses reveal core parasitism genes and suggest gene duplication and repurposing as sources of structural novelty. *Molecular Biology and Evolution* **32**, 767-790 (2015).
8. L. Wang *et al.*, The phytol phosphorylation pathway is essential for the biosynthesis of phylloquinone, which is required for photosystem i stability in *Arabidopsis*. *Molecular Plant* **10**, 183-196 (2017).
9. A. Fatihi *et al.*, A dedicated type II NADPH dehydrogenase performs the penultimate step in the biosynthesis of vitamin K1 in *Synechocystis* and *Arabidopsis*. *Plant Cell* **27**, 1730-1741 (2015).
10. L. Babujee *et al.*, The proteome map of spinach leaf peroxisomes indicates partial compartmentalization of phylloquinone (vitamin K1) biosynthesis in plant peroxisomes. *Journal of Experimental Botany* **61**, 1441-1453 (2010).
11. G. Schultz, J. Soll, B. H. Ellerbrock, Site of prenylation reaction in synthesis of phylloquinone (vitamin K1) by spinach chloroplasts. *European Journal of Biochemistry* **117**, 329-332 (1981).
12. S. Kaiping, J. Soll, G. Schultz, Site of methylation of 2-phytyl-1,4-naphthoquinol in phylloquinone (vitamin K1) synthesis in spinach chloroplasts. *Phytochemistry* **23**, 89-91 (1984).
13. N. Matasci *et al.*, Data access for the 1,000 Plants (1KP) project. *GigaScience* **3**, 17 (2014).
14. H. Shimada *et al.*, Inactivation and deficiency of core proteins of photosystems I and II caused by genetical phylloquinone and plastoquinone deficiency but retained lamellar structure in a T-DNA mutant of Arabidopsis. *Plant Journal* **41**, 627-637 (2005).
15. D. Kim, R. Kocz, L. Boone, W. John Keyes, D. G. Lynn, On becoming a parasite: evaluating the role of wall oxidases in parasitic plant development. *Chemistry & Biology* **5**, 103-117 (1998).
16. C. I. González-Verdejo, X. Barandiaran, M. T. Moreno, J. I. Cubero, A. Di Pietro, A peroxidase gene expressed during early developmental stages of the parasitic plant *Orobanche ramosa*. *Journal of Experimental Botany* **57**, 185-192 (2006).
17. C. Veronesi, E. Bonnin, S. Calvez, P. Thalouarn, P. Simier, Activity of secreted cell wall-modifying enzymes and expression of peroxidase-encoding gene following germination of *Orobanche ramosa*. *Biologia Plantarum* **51**, 391-394 (2007).
18. P. C. G. Bandaranayake *et al.*, A single-electron reducing quinone oxidoreductase is necessary to induce haustorium development in the root parasitic plant *Triphysaria*. *Plant Cell* **22**, 1404-1419 (2010).
19. A. Bérczi, I. M. Møller, Redox enzymes in the plant plasma membrane and their possible roles. *Plant Cell and Environment* **23**, 1287-1302 (2000).

20. J. W. Keyes, C. R. O'Malley, D. Kim, G. D. Lynn, Signaling organogenesis in parasitic angiosperms: Xenognosin generation, perception, and response. *Journal of Plant Growth Regulation* **19**, 217-231 (2000).
21. R. L. Wrobel, M. Matvienko, J. I. Yoder, Heterologous expression and biochemical characterization of an NAD(P)H:quinone oxidoreductase from the hemiparasitic plant *Triphysaria versicolor*. *Plant Physiology and Biochemistry* **40**, 265-272 (2002).
22. P. Schopfer, E. Heyno, F. Drepper, A. Krieger-Liszkay, Naphthoquinone-dependent generation of superoxide radicals by quinone reductase isolated from the plasma membrane of soybean. *Plant Physiology* **147**, 864-878 (2008).
23. J. K. Ishida *et al.*, Local auxin biosynthesis mediated by a YUCCA flavin monooxygenase regulates haustorium development in the parasitic plant *Phtheirospermum japonicum*. *Plant Cell* **28**, 1795-1814 (2016).
24. L. Liang, Y. Liu, J. Jariwala, D. G. Lynn, A. G. Palmer, Detection and adaptation in parasitic angiosperm host selection. *American Journal of Plant Sciences* **7**, 1275-1290 (2016).
25. A. Marmagne *et al.*, Identification of new intrinsic proteins in *Arabidopsis* plasma membrane proteome. *Molecular & Cellular Proteomics* **3**, 675-691 (2004).
26. A. Bridge, R. Barr, D. J. Morré, The plasma membrane NADH oxidase of soybean has vitamin K1 hydroquinone oxidase activity. *Biochimica et Biophysica Acta (BBA) - Biomembranes* **1463**, 448-458 (2000).
27. M. Bernal *et al.*, Transcriptome sequencing identifies SPL7-regulated copper acquisition genes FRO4/FRO5 and the copper dependence of iron homeostasis in *Arabidopsis*. *Plant Cell* **24**, 738-761 (2012).
28. J. H. Westwood, J. I. Yoder, M. P. Timko, C. W. dePamphilis, The evolution of parasitism in plants. *Trends in Plant Science* **15**, 227-235 (2010).
29. X. Gu, S. J. Queen, C.-J. Tsai, PLAS: Parallelized local assembly of next-generation sequences. https://github.com/TsailabBioinformatics/Scripts/tree/master/PLAS.
30. B. Langmead, S. L. Salzberg, Fast gapped-read alignment with Bowtie 2. *Nature methods* **9**, 357-359 (2012).
31. B. J. Haas *et al.*, *De novo* transcript sequence reconstruction from RNA-Seq: reference generation and analysis with Trinity. *Nature protocols* **8**, 10.1038/nprot.2013.1084 (2013).
32. A. Roberts, L. Pachter, Streaming fragment assignment for real-time analysis of sequencing experiments. *Nat Meth* **10**, 71-73 (2013).
33. I. Small, N. Peeters, F. Legeai, C. Lurin, Predotar: A tool for rapidly screening proteomes for N-terminal targeting sequences. *PROTEOMICS* **4**, 1581-1590 (2004).
34. O. Emanuelsson, S. Brunak, G. von Heijne, H. Nielsen, Locating proteins in the cell using TargetP, SignalP and related tools. *Nat. Protocols* **2**, 953-971 (2007).
35. M. Bodén, J. Hawkins, Prediction of subcellular localization using sequence-biased recurrent networks. *Bioinformatics* **21**, 2279-2286 (2005).
36. P. Horton *et al.*, WoLF PSORT: protein localization predictor. *Nucleic Acids Research* **35**, W585-W587 (2007).
37. A. Krogh, B. Larsson, G. von Heijne, E. L. L. Sonnhammer, Predicting transmembrane protein topology with a hidden markov model: application to complete genomes1. *Journal of Molecular Biology* **305**, 567-580 (2001).
38. B. Hu *et al.*, GSDS 2.0: an upgraded gene feature visualization server. *Bioinformatics* **31**, 1296-1297 (2015).
39. K. Katoh, D. M. Standley, MAFFT multiple sequence alignment software version 7: Improvements in performance and usability. *Molecular Biology and Evolution* **30**, 772-780 (2013).
40. A. Alexa, J. Rahnenführer, T. Lengauer, Improved scoring of functional groups from gene expression data by decorrelating GO graph structure. *Bioinformatics* **22**, 1600-1607 (2006).
41. D. M. Emms, S. Kelly, OrthoFinder: solving fundamental biases in whole genome comparisons dramatically improves orthogroup inference accuracy. *Genome Biology* **16**, 157 (2015).
42. P. Shannon *et al.*, Cytoscape: A software environment for integrated models of biomolecular interaction networks. *Genome Research* **13**, 2498-2504 (2003).
43. M. Martin, Cutadapt removes adapter sequences from high-throughput sequencing reads. *EMBnet.journal* **17**, 10-12 (2011).
44. A. M. Bolger, M. Lohse, B. Usadel, Trimmomatic: a flexible trimmer for Illumina sequence data. *Bioinformatics* **30**, 2114-2120 (2014).

45. D. Kim *et al.*, TopHat2: accurate alignment of transcriptomes in the presence of insertions, deletions and gene fusions. *Genome Biology* **14**, R36 (2013).
46. H. Li *et al.*, The Sequence Alignment/Map format and SAMtools. *Bioinformatics* **25**, 2078-2079 (2009).
47. S. Anders, P. T. Pyl, W. Huber, HTSeq—a Python framework to work with high-throughput sequencing data. *Bioinformatics* **31**, 166-169 (2015).
48. M. I. Love, W. Huber, S. Anders, Moderated estimation of fold change and dispersion for RNA-seq data with DESeq2. *Genome Biology* **15**, 550 (2014).
49. R. C. Edgar, MUSCLE: multiple sequence alignment with high accuracy and high throughput. *Nucleic Acids Research* **32**, 1792-1797 (2004).
50. J. Castresana, Selection of conserved blocks from multiple alignments for their use in phylogenetic analysis. *Molecular Biology and Evolution* **17**, 540-552 (2000).
51. F. Ronquist *et al.*, MrBayes 3.2: Efficient Bayesian phylogenetic inference and model choice across a large model space. *Systematic Biology* **61**, 539-542 (2012).
52. J. H. Westwood *et al.*, The Parasitic Plant Genome Project: New tools for understanding the biology of *Orobanche* and *Striga*. *Weed Science* **60**, 295-306 (2012).
53. S. Shahid *et al.*, MicroRNAs from the parasitic plant Cuscuta campestris target host messenger RNAs. *Nature* **553**, 82 (2018).
54. S. L. Booth, K. W. Davidson, J. A. Sadowski, Evaluation of an HPLC method for the determination of phylloquinone (vitamin K1) in various food matrixes. *Journal of Agricultural and Food Chemistry* **42**, 295-300 (1994).
55. S. Chen, P. Songkumarn, J. Liu, G.-L. Wang, A versatile zero background T-vector system for gene cloning and functional genomics. *Plant Physiol.* **150**, 1111-1121 (2009).
56. D. Peng, L.-J. Xue, X. Gu, J. H. Leebens-Mack, C.-J. Tsai, Bayesian phylogeny of sucrose transporters: Ancient origins, differential expansion and convergent evolution in monocots and dicots. *Frontiers in Plant Science* **5**, 615 (2014).
57. K. M. Pathi, S. Tula, N. Tuteja, High frequency regeneration via direct somatic embryogenesis and efficient *Agrobacterium*-mediated genetic transformation of tobacco. *Plant Signaling & Behavior* **8**, e24354 (2013).

Acknowledgments: We thank L.-J. Xue for the GCC Python script, M. Curley for preparation of the AtMenA.1-GFP construct, N. Rodman for *Nicotiana* transformation, J. Gordon for help with microscopy, M. Tsai, M. Ortega and V. Meneses for laboratory assistance, and D. Lynn for insightful discussion. This work was supported by Georgia Research Alliance-Hank Haynes Forest Biotechnology Endowment (C.-J.T.), National Science Foundation (IOS-1444567/C.-J.T. and IOS-1238057/J.H.W.), National Institute of Food and Agriculture (2015-67013-22812/C.-J.T. and VA-135997/J.H.W.), and University of Georgia Graduate School's Innovative and Interdisciplinary Research Grant (X.G.). C.-J.T and X.G. conceived the study; X.G. performed all molecular analyses with inputs from C.-J.T.; S.A.H, B.N., and K.B.A. provided technical assistance; K.C. and J.H.W. contributed materials; X.G. and C.-J.T. wrote the manuscript with contributions from S.A.H and J.H.W.

Supplementary Materials:

Transcriptome assembly of parasitic plants

RNA-Seq data of *Phelipanche aegyptiaca*, *Striga hermonthica* and *Triphysaria versicolor* were downloaded from the Parasitic Plant Genome Project database (http://ppgp.huck.psu.edu/). Raw data were pre-processed using in-house scripts to remove adapters, non-coding RNAs, low-quality and low-complexity reads. Cleaned reads were assembled using a custom Parallelized Local Assembly of Sequences (PLAS) pipeline (*29*). Briefly, PLAS performs reference-guided read mapping using Bowtie 2 v2.2.3 (*30*) against a closely related proteome (*Mimulus guttatus*) binned by homology to facilitate parallel computing. Mapped reads were used for *de novo*

assembly by Trinity (*31*), and the assembled contigs were quality-checked against the reference in each bin by Blast before being used as baits in the next round of *de novo* assembly. This process was repeated for up to 10 iterations until the output was stable. Assembled sequences were filtered to remove potential contaminations (*e.g.*, host plants, protozoa, invertebrates, bacteria, fungi and human sequences) and redundant contigs sharing at least 95% sequence identity. The transcriptome was annotated against the *A. thaliana* proteome, *M. guttatus* proteome and Uni-Prot database. Transcript abundance was estimated using eXpress 1.5.1 (*32*). Additional MenA and MenG sequences were obtained from the 1000 Plants database (*13*) by Blast (https://db.cngb.org/blast4onekp/) against the 'Core Eudicots/Asterids' clade using *P. aegyptiaca* sequences as query.

Subcellular and transmembrane domain prediction and gene structure

PhQ gene sequences of photosynthetic species were downloaded from Phytozome v11 (https://phytozome.jgi.doe.gov). Subcellular localization was predicted by Predotar 1.04 (*33*), TargetP 1.1 (*34*), Protein Prowler 1.2 (*35*), and WolF PSORT (*36*). Transmembrane domain was predicted by TMHMM Server v.2.0 (*37*), and data plotted in *R*. Gene structures were drawn by Gene Structure Display Server 2.0 (*38*). The exon-intron junctions of parasitic *MenA* and *MenG* were inferred by Blast alignment of transcripts against genomic short read data of *Phelipanche* (NCBI Sequence Read Archive accession SRX2067908), *Striga* (SRX2067907) and *Triphysaria* (SRX973263). Sequence alignment was performed using MAFFT (*39*) and visualized with Color Align Conservation (www.bioinformatics.org/sms2/color_align_cons.html).

Co-expression analysis

Transcripts with an FPKM ≥2 in at least two samples were subject to pair-wise Gini Correlation Coefficient (GCC) computation using a python script. PhQ-coexpressed transcripts were defined as the 500 most highly correlated transcripts or those with a GCC ≥0.8 for each PhQ pathway gene. The union sets were used for Gene Ontology enrichment analysis using topGO R package 2.26.0 (*40*). To facilitate comparative analysis between the three parasitic species, ortholog groups were constructed by OrthoFinder 1.0.8 (*41*). Network visualization was performed in Cytoscape 3.4.0 (*42*) using edge-weighted spring embedded layout, with a GCC cutoff of 0.6.

RNA-seq data processing of photoautotrophic species

RNA-seq data of *A. thaliana*, *Glycine max* and *Populus tremula* × *alba* were downloaded from the NCBI SRA and processed by Cutadapt 1.9.dev1 (*43*), Trimmomatic 0.32 (*44*) and custom scripts to remove adapter, low-quality reads, rRNA and organellar sequences. Reads were mapped by Tophat 2.0.13 (*45*), alignment sorted by Samtools 1.2 (*46*), and read count and expression estimation obtained by HTseq 0.6.1p1 (*47*) and DESeq2 (*48*). *A. thaliana* data used for GCC computation (excluding stressed samples) were SRA236885, SRA091517, SRA269936, SRA219425, SRA308579, SRA050132, SRA067724, SRA291734, SRA269101, SRA098075, SRA100242, SRA122395, SRA163488, SRA064368, SRA246225, SRA248861, SRA202878, SRA201550, SRA303151, SRA221137, SRA272654, and SRA221060. *G. max* data included SRA187830, SRA047293, SRA036577, SRA116533, SRA091756, SRA187830, SRA036538, SRA036577, and SRA129337. *P. tremula* × *alba* datasets were SRA274261 and SRA097208.

Phylogenetic tree construction

The protein sequences of *P. ramosa* OrPRX1 (AAY89058) and OrPOX1 (AAU04440), and *S. asiatica* SaPOXA (AAB97853) and SaPOXB (AF043235) were searched against the transcriptome assemblies of *P. aegyptiaca*, *S. hermonthica* and *T. versicolor* to identify

orthologs. Their protein sequences were aligned by MUSCLE 3.8.31 (*49*) and the alignment trimmed by Gblocks (*50*). Bayesian phylogenetic tree was constructed using MrBayes 3.2.5 (*51*).

PhQ analysis

P. aegyptiaca seeds were surface-sterilized, pre-conditioned on moist filter paper for 7-10 days, and treated with GR-24 for 4-6 days before collection of stage 1 seeds with radicle growth as described (*52*). *C. campestris* (previously published as *C. pentagona*, a highly similar species; see *53*) seeds were sterilized and germinated on moist filter paper for 6 days before sampling. Non-imbibed *A. thaliana* (Col-0) seeds were used without further treatment. Tissues were snap-frozen in liquid nitrogen, freeze-dried and milled to a fine powder for PhQ analysis as described (*54*). Tissues were partitioned twice in isopropanol/hexane (3:2 v/v), with menaquinone MK-4 (Sigma V9378) as internal standard for *P. aegyptiaca* analysis. The hexane phase was dried under nitrogen, and resuspended in methylene chloride:methanol (1:4, v/v), 10 mM ZnCl2, 5mM Na-acetate, and 5 mM acetic acid. Isocratic reverse-phase chromatography (Agilent Eclipse Plus C18 column, 5 µm 4.6x250 mm) was carried out using methanol:methylene chloride (9:1, v/v), with post-column Zn reduction and fluorescence detection (excitation 244 nm, emission 418 nm).

Nicotiana benthamiana transformation and confocal microscopy

AtMenA.1 cDNA (from the Arabidopsis Biological Resource Center) corresponding to the N-terminal truncated splice isoform was PCR amplified using gene-specific oligos with homology extensions matching 35S promoter (lower case, 5'-caatcaagcattctacttctagATGTACTCTGTCGCTTTAGTTC, *Xba*I site is underlined) or GFP (italic, 5'-*AAAGTTCTTCTCCTTTACCCAT*TCTAGAGCGCGCGATAACTAGCCCCAA). GFP coding sequence was PCR amplified from pCX-DG vector (*55*) using 5'-ATGGGTAAAGGAGAAGAACTTT and 5'-gaacgatcggggaaattcgCTATCTGGCTTTTAGTAAGCCCC (lower case matching NOS terminator). PCR fragments were column-purified using the DNA Clean and Concentrator™-5 kit (Zymo Research), and Gibson assembled into *Bam*HI-digested pCXSN vector (*55*) using the NEBuilder HiFi DNA Assembly Cloning Kit (New England Biolabs). The resulting pCX-AtMenA.1-GFP construct was sequence-verified. *PaMenA* and *PaMenG* coding sequences were gene-synthesize (General Biosystems) and subcloned into *Xba*I-digested pCX-AtMenA.1-GFP vector to generate pCX-PaMenA-GFP and pCX-PaMenG-GFP, respectively. A GFP fusion construct of a tonoplast sucrose transporter from *Amborella trichopoda* (*56*) was also included as a control. *Agrobacterium*-mediated transformation of *Nicotiana benthamiana* was performed as described and regenerated on selection media (*57*). Primary transformants were confirmed by PCR using primers for selectable marker hygromycin phosphotransferase (5'-GAGGGCGAAGAATCTCGTGC and 5'-GATGTTGGCGACCTCGTATTGG) or for genes of interest with a 35S promoter primer (5'-CCCACTATCCTTCGCAAGACC) and a gene-specific primer (PaMenA, 5'-CCTCAAGAGCTACCCAACAAAG; PaMenG, 5'-CGACATGCAGCGACCTGTAATA; and AtMenA.1, 5'-TCCGGCTTCCAACCAGATTTA). Leaf samples from PCR-positive transformants were imaged using a Keyence BZX-700 fluorescence microscope.